Rainfall erosivity mapping in mainland China using 1-minute precipitation data from densely distributed weather stations

Yueli Chen[1], Yun Xie[2], Xingwu Duan[3], Minghu Ding[1]

[1]State Key Laboratory of Severe Weather, Chinese Academy of Meteorological Sciences, Beijing, 100081, China
5 [2]College of Arts and Sciences, Beijing Normal University at Zhuhai, Zhuhai, 519087, China
[3]Institute of International Rivers and Eco-security, Yunnan University, Kunming, 650091, China

Correspondence to: Yueli Chen (chenylchina@yeah.net) and Yun Xie (xieyun@bnu.edu.cn)

Abstract. The risk of water erosion in mainland China is intensifying due to climate change. A high-precision rainfall erosivity dataset is crucial for understanding the spatiotemporal patterns of rainfall erosivity and identifying key areas of
10 water erosion. However, due to the limited spatiotemporal resolution of historical precipitation data, there are significant biases in the estimation of rainfall erosivity in China, particularly in regions with complex terrain and climatic conditions. Over the past decade, the China Meteorological Administration has continuously strengthened its ground-based meteorological observation capabilities, establishing a dense network of observation stations. These high-precision precipitation data provide a reliable basis for quantifying rainfall erosivity pattern in China. In this study, rigorous quality
15 control was performed on the 1-minute ground observation precipitation data from nearly 70,000 stations nationwide between 2014 and 2022, ultimately selecting data from 60,129 stations. Using the data from these stations, event rainfall erosivity was calculated, producing a national dataset of mean annual rainfall erosivity with a spatial resolution of 0.25°. This dataset shows that the mean annual rainfall erosivity in mainland China is approximately 1241 MJ·mm·ha^{-1}·h^{-1}·yr^{-1}, with values exceeding 4000 MJ·mm·ha^{-1}·yr^{-1} primarily concentrated in southern China and the southern Tibetan Plateau.
20 The mean annual rainfall erosivity in mainland China derived from previously released datasets was found to be 31% to 65% higher than the value calculated in this study, and basin-level discrepancies between our findings and other studies also varies significantly. In summary, the release of this dataset enables a more accurate assessment of the current intensity of water erosion in China. The dataset is available from the National Tibetan Plateau/Third Pole Environment Data Center (https://doi.org/10.11888/Terre.tpdc.301206; Chen, 2024).

1 Introduction

Rainfall-induced soil erosion is a primary contributor to global soil loss, as highlighted by the Intergovernmental Panel on Climate Change (IPCC, 2019), posing a significant threat to soil functionality. This phenomenon jeopardizes various crucial aspects, including food security, water quality, and climate change mitigation (FAO and IPTS, 2015; Panagos et al. 2020). Precipitation is the principal driver of erosion processes, influencing soil particle detachment, aggregate breakdown, and
30 particle transport via runoff (Wischmeier and Smith, 1965, 1978). In this context, the rainfall erosivity index was introduced

to quantify the potential of rainfall to cause soil loss, particularly using the Universal Soil Loss Equation (USLE), which links rainfall characteristics to soil loss based on extensive data from thousands of plot-years of natural rainfall and runoff (Nearing et al., 2017). In recent years, rainfall erosivity has also been widely used in assessing ecosystem service functions, post-fire debris flows, and other environmental hazards (Diodato et al., 2020; McGuire et al., 2024; Wu et al., 2024).

35 Rainfall erosivity is commonly assessed by multiplying the accumulated kinetic energy (E) by the maximum 30-minute rainfall intensity (I_{30}) of a rainfall event. From a dynamic perspective, this index encapsulates the comprehensive effects of soil particle detachment and transport processes. The E of a rainfall event can be quantified using the raindrop physical parameters such as raindrop size and falling velocity measured using distrometers. However, it is challenge to obtain these parameters on a large spatial scale due to the high cost of maintaining a dense observational network of distrometers. To
40 simplify the calculation, empirical models relating E to rainfall intensity (I) (hereafter referred to as the E-I relation) are developed based on observed raindrop fall velocity and size to estimate the E of rainfall events. The common used forms of E-I relation models include polynomial (Carter et al., 1974; Tilg et al., 2020), exponential (Kinnell, 1980; Brown and Foster, 1987; Renard et al., 1997; Mineo et al., 2019), logarithmic (Wischmeier and Smith, 1958, 1978; Davison et al., 2005), and power-law (Laws, 1941; Laws and Parsons, 1943; Uijlenhoet and Stricker, 1999; Lim et al., 2015) equations, etc. It is
45 important to note that the accuracy of E depends not only on the models used but also on the temporal resolution of the in-situ precipitation observations, considering the non-linear E-I relationship. For example, for logarithmic and exponential E-I relation models, like those used in the USLE and Revised Universal Soil Loss Equation (RUSLE), studies have shown that E values derived from 1-hour in-situ precipitation data are about 10% lower than those derived from 1-minute data (Agnese et al., 2006; Yin et al., 2007). In 2023, Dai et al. (2023) introduced the first global rainfall microphysics-based E values
50 retrieved from radar reflectivity at different frequencies, showing that microphysics-based E estimates outperform those derived from commonly used empirical KE-I relations, validated using ground disdrometers. Specifically, the mean annual rainfall kinetic energy calculating using the E-I method was found to be 6.17% to 12.5% lower than the radar remote sensing-based E values across distinct regions worldwide.

The I_{30} value of a rainfall event is derived from precipitation process data, including both in-situ and gridded precipitation
55 data. In-situ precipitation data with 1-minute temporal resolution are the best suitable data for deriving I_{30} of a rain event. Precipitation data with a temporal resolution greater than 15-minute may fail to capture the accurate sub-hourly rainfall process, resulting in underestimated I_{30} values (Angulo-Martínez and Beguería, 2009). For example, the I_{30} value derived from 1-minute data is found to be approximately1.668 times higher than that derived from hourly records in mainland China (Yin et al., 2007). As remote sensing technology and weather forecasting models advance, the temporal resolution of gridded
60 precipitation data has greatly improved, allowing their use to derive I_{30} values. However, caution is needed, as I_{30} values may be underestimated when using gridded precipitation data. For example, the European Center for Medium-Range Weather Forecasts Reanalysis 5 (ERA5) reanalysis precipitation data underestimates I_{30} values by over 80% in the Tibetan Plateau (Chen et al., 2022). Satellite-based products, such as the Integrated Multi-satellitE Retrievals for the Global Precipitation Measurement (GPM, IMERG) dataset, also show significant underestimations in precipitation intensity, posing challenges in

65   accurately identifying I_{30} (Freitas et al., 2020).

Based on the analysis, the variation among different E estimates derived from different data sources and methods is around 10%. In contrast, the bias in I_{30} estimates from precipitation data with varying temporal resolutions exceeds 60%. The bias in I_{30} for individual rainfall event is significantly great than that for E. Therefore, the I_{30} estimation bias is the crucial source of inaccuracies in determining rainfall erosivity. The most reliable approach for obtaining I_{30} and corresponding rainfall

70   erosivity values is to use in-situ observations from densely spaced weather station networks.

Due to the limited availability of high temporal-spatial resolution precipitation data, rainfall erosivity in China has traditionally been estimated using coarser resolution precipitation data (limited in-situ records and gridded data), such as hourly, daily, monthly, or yearly scales (Yin et al., 2015; Panagos et al., 2017; Liu et al., 2020; Yue et al., 2022; Chen et al., 2022, 2023). Consequently, existing maps of mean annual rainfall erosivity (hereafter referred to as the R factor) may

75   contain significant uncertainties, particularly in regions with complex terrain and climate conditions (Chen et al., 2022). Since 2012, the China Meteorological Administration (CMA) has developed a dense network of automatic weather stations, providing 1-minute in-situ precipitation records nationwide. This development offers an opportunity to better identify sub-hourly rainfall characteristics. By leveraging this dataset, accurate I_{30} values, event rainfall erosivity, and mean annual rainfall erosivity for the recent decade in mainland China can be obtained. This study aims to: 1) determine R factor values at

80   approximately 70,000 weather stations using the standard method; 2) develop an R factor map for mainland China by integrating values based on 1-minute in-situ data with those derived from hourly ERA5 reanalysis precipitation data; 3) identify the sources of uncertainties in estimating the R factor.

2 Data and methods

2.1 Data

85   **2.1.1 Precipitation data**

Over the past decade, approximately 70,000 weather stations have been established by the CMA, maintaining nearly 10 years of precipitation observations at 1-minute intervals. To ensure the accuracy of these in-situ data, the quality of records was evaluated using a data integrity index, defined as the ratio of available records to the total number of minutes in a year for each station. Records with an integrity level above 90% for a given year were deemed suitable for calculating annual

90   rainfall erosivity at the respective stations. Ultimately, data from 60,129 stations across the mainland China spanning 2014-2022 were used in this study.

Mainland China was divided into 16,167 grids with a spatial resolution of 0.25°. Based on this division, we analyzed the density of weather stations and the length of available data coverage at the grid scale (Figure 1). Results indicated that the density of stations and coverage time length were significantly higher in the southeastern regions of China compared to the

95   northwest. On a national scale, approximately 57% of all grids had in-situ precipitation observation, with an average of 6.7 stations per grid and data coverage of 5.2 years.
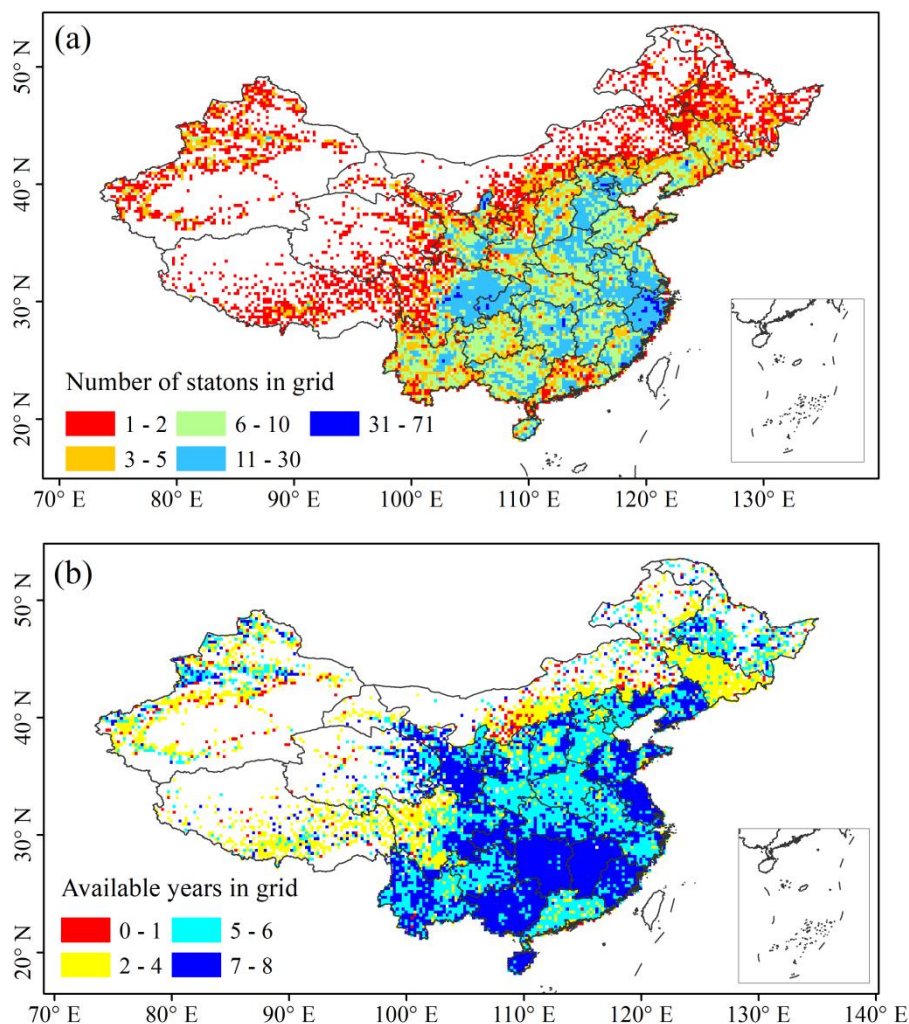
Figure 1: (a) Number of available weather stations and (b) averaged coverage time length of in-situ precipitation records in each 0.25° grid across mainland China.

A monthly gridded precipitation dataset, released by the National Meteorological Information Center (NMIC) of the CMA, was also employed to analyze the spatial characteristics of precipitation across China (hereafter referred to as the CMA gridded precipitation data). This dataset was particularly valuable for regions with insufficient station data, such as northwestern China. The gridded precipitation dataset is based on national weather station data and interpolated into 0.5° grids using the Thin Plate Spline method. This study used data from 2014 to 2022 to detect the spatial characteristics of multi-year averaged annual precipitation across China.

The hourly 0.25° ERA5 reanalysis precipitation dataset was employed to calculate rainfall erosivity in the Dawang-Chayu

area, located in the southern part of the Tibetan Plateau, which receives more than 1,000 mm of annual precipitation but lacks 1-minute precipitation records. ERA5 precipitation data include large-scale and convective precipitation consisting of rain and snow, produced by the European Center for Medium-Range Weather Forecasts Integrated Forecasting System. This dataset, representing the latest generation of global atmospheric reanalysis, provides a higher spatial resolution compared to ERA-Interim (Hersbach et al., 2019).

2.1.2 Rainfall erosivity maps in previous studies

The newly developed R factor map for mainland China, presented in the results section, is compared with previous studies. Two widely used R factor maps from Panogos et al. (2017) and Yue et al. (2022) were selected for comparison. Panogos et al. (2017) developed the first global-scale rainfall erosivity database using hourly in-situ precipitation records from 3,625 stations spread across 63 countries (https://esdac.jrc.ec.europa.eu/themes/global-rainfall-erosivity). The distribution of stations varies by continent, with Asia and the Middle East accounting for 1,220 stations (34% of the total) across 10 countries, including parts of Russia, China, India, and Japan. Yue et al. (2022) used hourly rainfall data from 2,381 stations between 1951 and 2018 to generate an R factor map for mainland China. This study demonstrated satisfactory performance by comparing derived values against true rainfall erosivity values calculated from 1-minute rainfall data collected from 62 stations across China. In this study, the overall performance of different R factor maps is first compared using grid-to-grid approach. Secondly, performance by basin is also assessed. Mainland China is divided into nine basin: the Songhua and Liaohe River Basin, Haihe River Basin, Huaihe River Basin, Yellow River Basin, Yangtze River Basin, Pearl River Basin, Southeast Basin, Southwest Basin, and Continental Basin (Figure 5a, https://www.resdc.cn/data.aspx?DATAID=141, last access 16 October 2024).

2.2 Method for calculating rainfall erosivity

Not all rainfall processes lead to soil erosion, and it is generally believed that rainfall must exceed a certain magnitude to cause soil erosion. According to Wischmeier and Smith (1978), a continuous six-hour dry period without any rainfall is used to delineate individual rainfall events. If rainfall is interrupted for more than six hours, subsequent rainfall is considered a separate event. Erosive rainfall events are defined as those with precipitation exceeding 12 mm (Xie et al., 2000). The rainfall erosivity (EI_{30}) of an erosive rainfall event is calculated according to the method proposed by Brown and Foster (1987), as recommended in RUSEL:

$$e_r = 0.29[1 - 0.72\exp(-0.05i_r)] \quad (1)$$

$$E = \sum_{r=1}^{n}(e_r \cdot P_r) \quad (2)$$

$$r_{event} = E \cdot I_{30} \quad (3)$$

where E (MJ·ha^{-1}) is the total energy of the erosive event, and r_{event} (MJ·mm·ha^{-1}·h^{-1}) is the event rainfall erosivity. For 1-

minute in-situ precipitation data, i_r (mm/h) is the rainfall intensity for the rth minute, e_r (MJ·ha^{-1}·mm^{-1}) is the unit energy for the rth minute, P_r (mm) is the rainfall amount for the rth minute, n is the rainfall duration in minutes, and I_{30} (mm/h) is the maximum contiguous 30-minute peak intensity.

To address occasional observation errors, particularly in low-temperature environments, a quality check was conducted on the calculated event rainfall erosivity. For each station, the nearest 100 stations were selected, and the recorded events at these 101 stations were categorized into two classifications: those occurring during the warm season (April to October) and those during the cold season (including months from January to March and November to December). The median and standard deviation of event rainfall erosivity were computed separately for both seasons. The threshold value for each station was defined as the median plus three times the standard deviation. Any event rainfall erosivity exceeding the threshold for the respective season was considered an outlier and excluded from the annual rainfall erosivity calculation. Ultimately, annual rainfall erosivity at each station was aggregated using quality-checked event rainfall erosivity values, with the R factor representing the mean annual rainfall erosivity. The R factor for a grid represents the multi-station averaged value. The overall algorithm for mapping R factor in mainland China is shown in Figure 2.
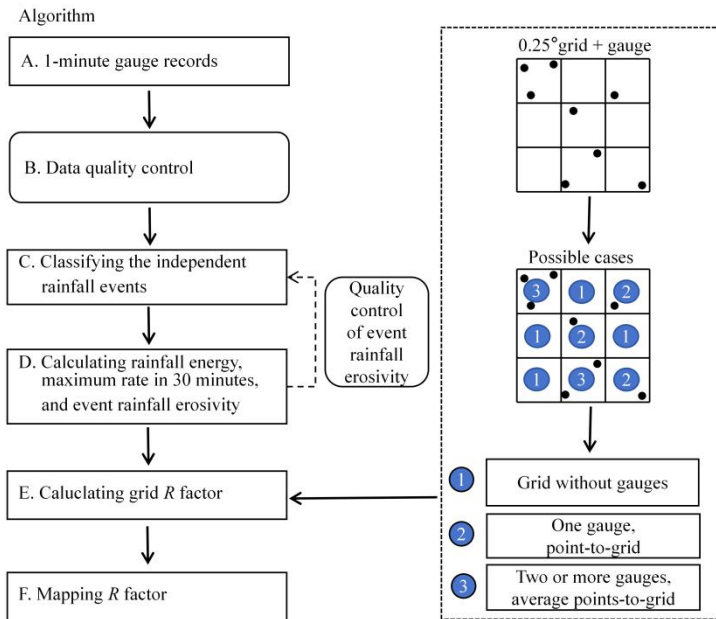
Figure 2. The algorithm for mapping R factor in mainland China

3 Results

3.1 Rainfall erosivity map

Using the methodology described in Section 2.2, the rainfall erosivity of erosive rainfall events was calculated for 60,129

stations across mainland China from 2014 to 2022. The R factor for each station was subsequently obtained, and gridded R
factor values were determined at a spatial resolution of 0.25°, representing the average R factor values of the stations within
corresponding grids (Figure 3). The averaged R factor across grids with in-situ observations in mainland China is 1,917
MJ·mm·ha^{-1}·h^{-1}·yr^{-1}. Overall, the southern region of China exhibits the highest mean annual rainfall erosivity, followed by
the northern region. The R factor is lowest in the arid and semi-arid areas of the northwest, as well as in the Tibetan Plateau.
In the southern region, the R factor generally exceeds 2,200 MJ·mm·ha^{-1}·h^{-1}·yr^{-1}, with the highest values observed along the
southeast coast, reaching over 10,000 MJ·mm·ha^{-1}·h^{-1}·yr^{-1}. In contrast, the R factor in the northwest and Tibetan Plateau
regions is mainly below 500 MJ·mm·ha^{-1}·h^{-1}·yr^{-1}.
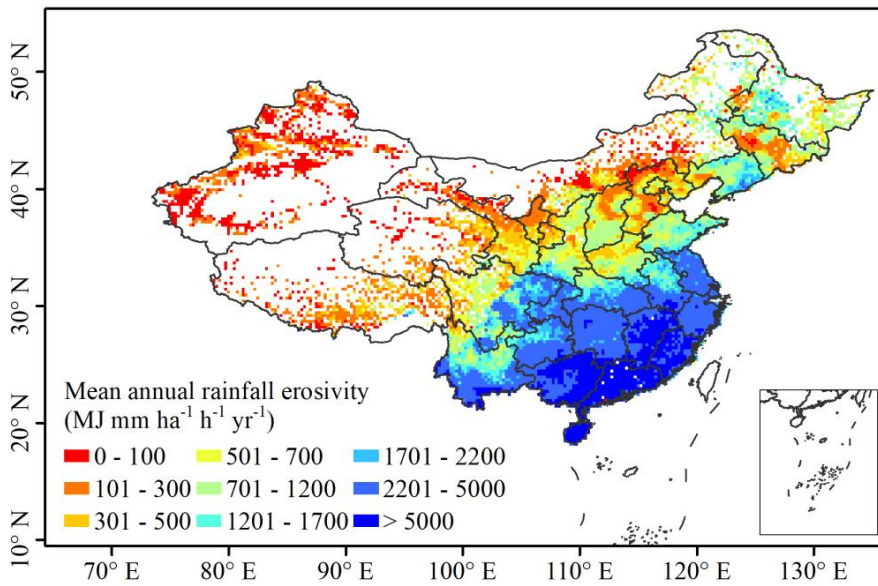
Figure 3: Mean annual rainfall erosivity (R factor) map

A spatial distribution map of the R factor across mainland China, with a spatial resolution of 0.25°, was generated using the Kriging method. Notably, large areas in the northwest and Tibetan Plateau lack ground observations, necessitating an assessment of the impact of spatial interpolation method on the accuracy of the R factor map in these regions. Given the

175 strong positive correlation between the R factor and annual precipitation (Richardson et al., 1983; Renard & Freimund, 1994; Yu et al., 1996; Xie et al., 2016; Chen et al., 2024), mean annual precipitation data were used to identify regions with high precipitation but no 1-minute records. Figure 4a shows the spatial distribution of mean annual precipitation deriving from CMA gridded precipitation data. Most observation gaps in the northwest and Tibetan Plateau have relatively low annual precipitation, with minimal differences compared to surrounding areas with observations. However, the Dawang-Chayu area,

180 located in the southern part of the Tibetan Plateau near the Yarlung Zangbo River Grand Canyon, is an exception. Precipitation in this region is primarily influenced by the southwest monsoon, which brings warm and humid airflow to the Tibetan Plateau (Chen et al., 2023). The observed mean annual precipitation here exceeds 1,800 mm, significantly higher than that in surrounding areas. Therefore, extrapolating rainfall erosivity from surrounding stations for this area is not reasonable.

185 To address this, hourly ERA5 reanalysis precipitation data, combined with in-situ precipitation records, were used to generate a gridded dataset of annual rainfall erosivity for the Tibetan Plateau from 1950 to 2020 (Chen et al., 2022). The mean annual rainfall erosivity for the Dawang-Chayu area from 2014 to 2022 was obtained form this dataset instead of relying on direct interpolation. Figure 4b shows the integrated R factor map for mainland China. Generally, the R factor in mainland China exhibits a decreasing trend from southeast to northwest, with an overall average value of 1,241

190 $MJ \cdot mm \cdot ha^{-1} \cdot h^{-1} \cdot yr^{-1}$.
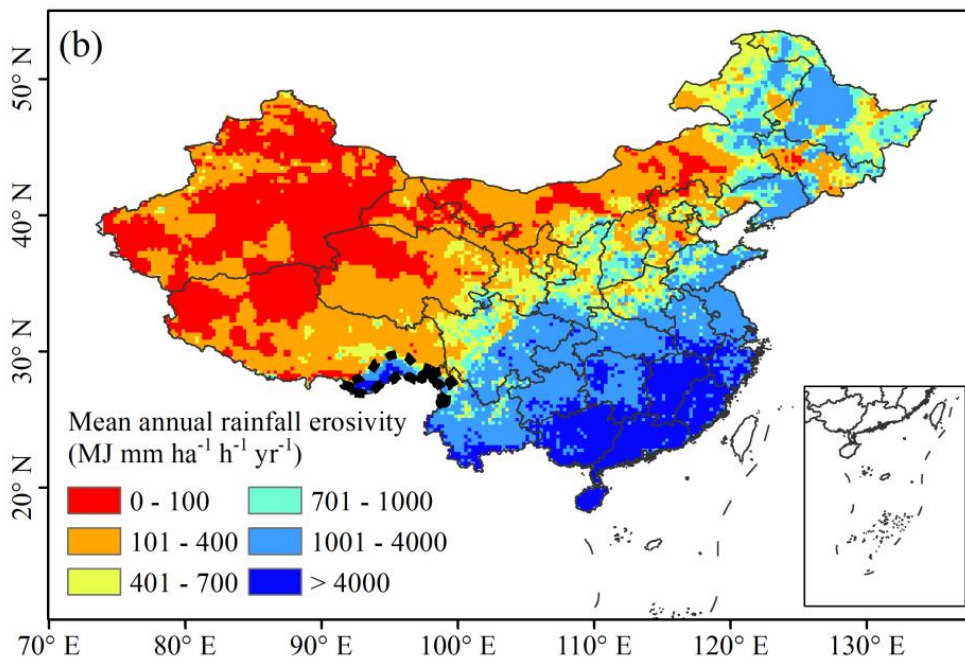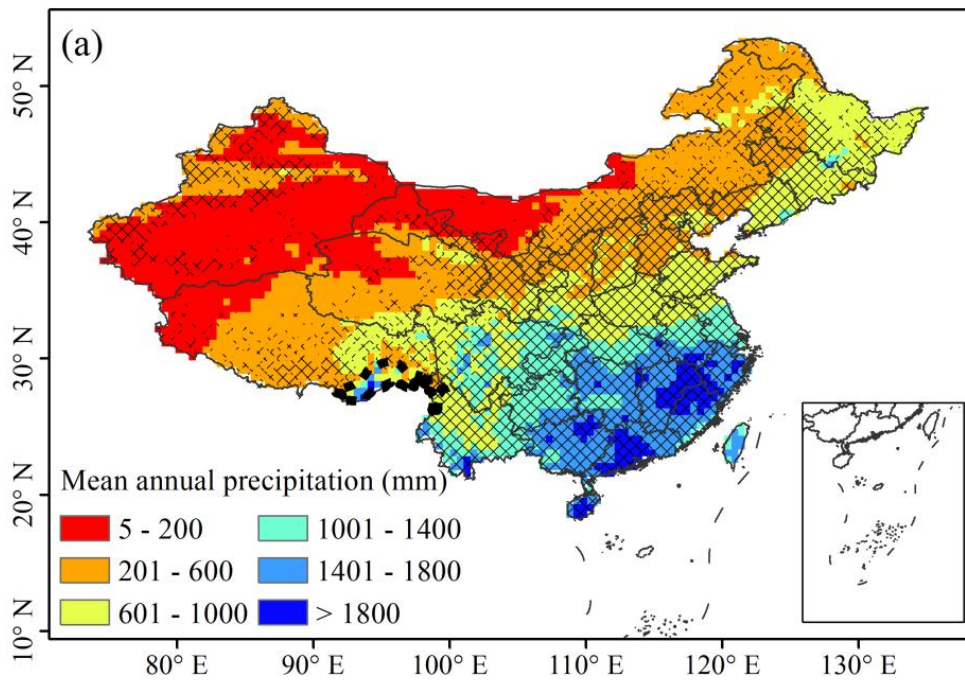
Figure 4: (a) Spatial distribution of mean annual precipitation in China. Grids without crossed diagonal lines indicates areas without station records. The black dashed line marks the Dawang-Chayu region. (b) Spatial distribution of *R* factor across mainland China.

3.2 Comparison with previous studies

The newly generated R factor map for mainland China is compared with the widely used maps from Panagos et al. (2017) and Yue et al. (2022) . Compared to the map developed by Panagos et al. (2017), there is a good correlation in regions with mean annual rainfall erosivity below 10,000 MJ·mm·ha^{-1}·h^{-1}·yr^{-1}. However, in areas with annual rainfall erosivity exceeding 10,000 MJ·mm·ha^{-1}·h^{-1}·yr^{-1}, our estimates are significantly higher (Figure 5a). When compared with the map by Yue et al. (2022), the overall correlation is good with annual rainfall erosivity less than 10,000 MJ·mm·ha^{-1}·h^{-1}·yr^{-1}. In regions with mean annual rainfall erosivity exceeds 10,000 MJ·mm·ha^{-1}·h^{-1}·yr^{-1}, the differences are larger, but no clear pattern is observed (Figure 5b). In summary, our results correlate well with existing studies in areas with lower mean annual rainfall erosivity but show significant differences in high-erosivity areas.
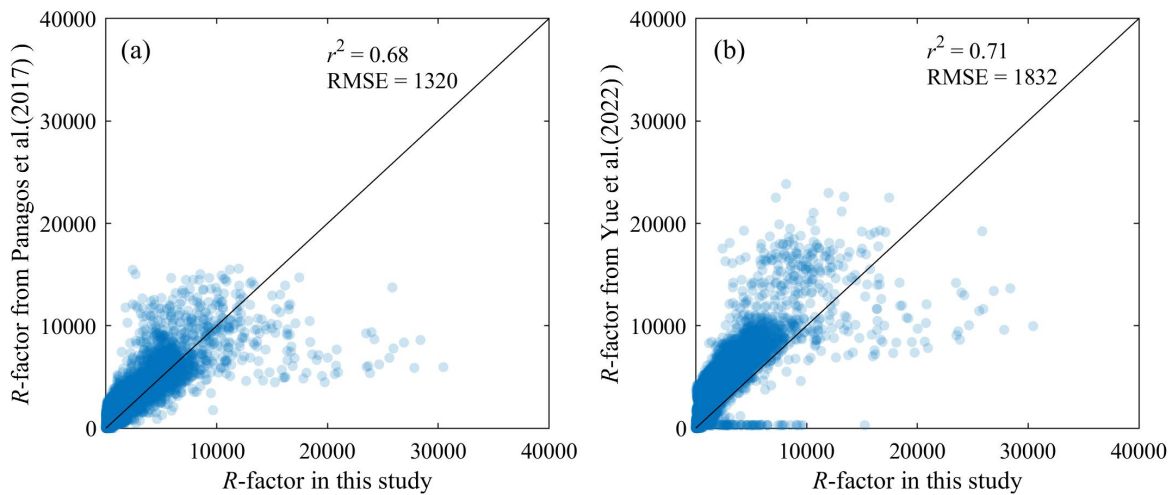
Figure 5: Comparisons between the newly developed R factor map and existing maps (Panagos et al., 2017; Yue et al., 2022).

A further comparison was conducted across the nine river basins in China (Figure 6). The Haihe and Huaihe River Basins show the largest differences in mean and median R factor values among the three datasets. Although some differences in performance are observed between basins, no consistent pattern emerge. These discrepancies primarily stem from variations in spatial and temporal resolution of the precipitation data and the algorithms used (Table 1). The algorithms in these studies are based on recommendations from RUSLE and RUSLE2. The E calculations of RUSLE are approximately 12% lower than those from RUSLE2 for precipitation intensities below 35 mm/hr, but 2% higher for intensities above 100 mm/hr (Nearing et al., 2017). Regarding I_{30}, 1-hour precipitation data cannot accurately capture this value. Unlike other studies, this research utilized the largest set of in-situ precipitation records but over a shorter time coverage. Since the R factor typically describes the potential of precipitation to cause erosion over a long-term climate scale, ideally spanning 20 years (Renard et al., 1997), using short-term data may introduce bias. Ayat et al. (2022) reported an increasing trend of extreme sub-hourly rainfall near

Sydney, Australia, over the last two decades, though no similar evidence exists for hourly or daily scales. However, trends in extreme sub-hourly rainfall over mainland China remain unclear. This study provides the *R* factor map for the past decade,

220 acknowledging potential biases, particularly in the context of climate change.
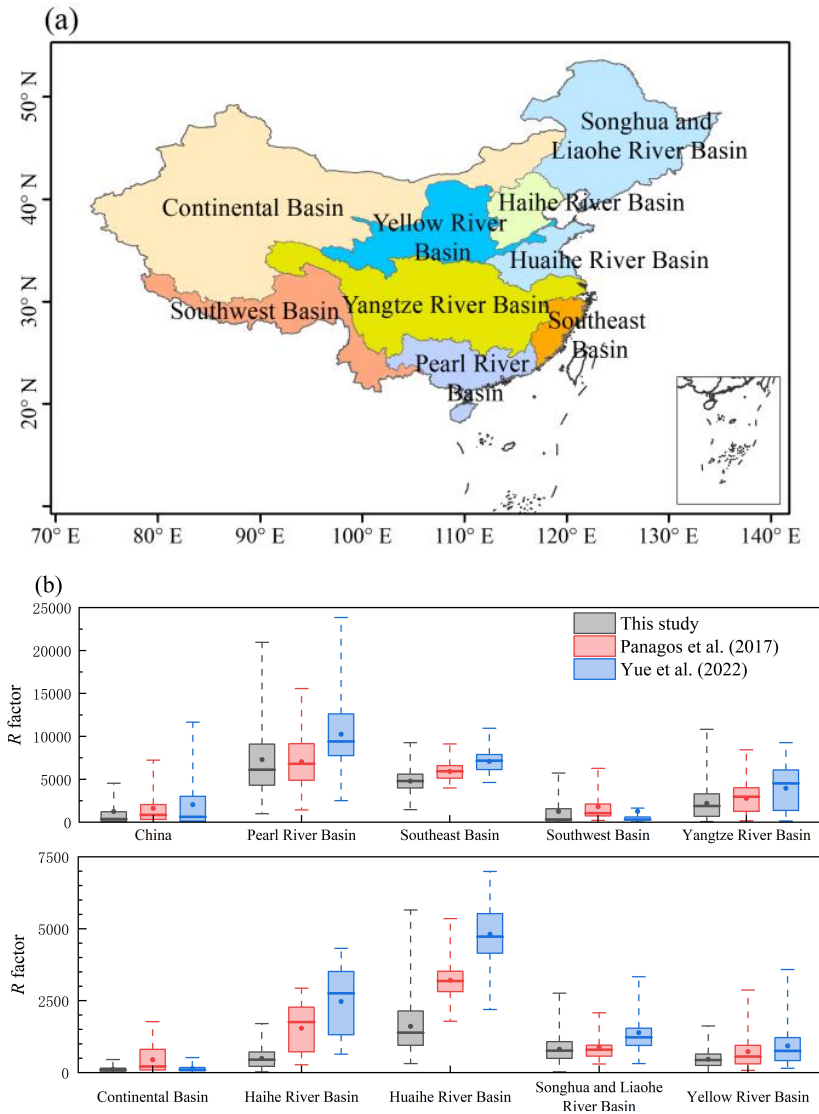
Figure 6: (a) The nine basins in China; (b) Box-plots of *R* factor across basins. Grey, red, and blue boxes represent different *R*
225 **factor maps from this study, Panagos et al. (2017), and Yue et al. (2022), respectively.**

Table 1 Comparison of data and methods used to generate *R* factor maps

R factor map	Temporal resolution of precipitation data	Number of stations	Time coverage	*E* algorithm	I_{30} (EI_{30}) algorithm	Spatial interpolation method
Panagos et al. (2017)	1-hour	387	14 years	RUSLE (Renard et al., 1997)	Conversion factor for *R* factor	Gaussian Process Regression
Yue et al. (2022)	1-hour	2381	18 to 54 years	RUSLE2 (USDA-Agricultural Research Service, 2013)	Conversion factor for *R* factor	Kriging
This study	1-minute	60129	9 years	RUSLE (Renard et al., 1997)	No conversion	Kriging

230

4. Impacts of precipitation data and algorithms on estimating rainfall erosivity

Variations in rainfall erosivity data and algorithms are the primary reasons for discrepancies in rainfall erosivity estimation. In this section, *E* values for erosive precipitation events are calculated using the kinetic energy methods from RUSLE and RUSLE2, evaluating how different kinetic energy algorithms affect rainfall erosivity estimation. To assess the impact of

235   temporal resolution of precipitation data on the accuracy of I_{30}, I_{30} values for erosive rainfall events were calculated using precipitation data at different temporal resolutions (1-minute vs. 1-hour). A total of 300 stations across China were randomly selected, using minute-level and hour-level precipitation data from 2020-2022 for comparison.

Figure 7 (a) and (b) show the mean *E* and I_{30} for erosive rainfall events across mainland China during 2020-2022. The mean event *E* value is 6.2 MJ/ha, ranging from 1.8 to 12.5 MJ/ha, and shows a decreasing trend from southeast to northwest. The

240   mean event I_{30} value is 18.9 mm/h, ranging from 3.0 to 34.9 mm/h, with two notable centers in the southern and central parts of China (Beijing-Tianjin-Hebei region, Shanxi, Henan, and Shandong provinces). Next, the differences between *E* computation using RUSLE and RUSLE2 were analyzed. For minute-level data, the ratio of the average event kinetic energy computed using RUSLE2 to RUSLE is approximately 1.09, while it is 1.15 for hourly data (Figures 7c and 7d). Next, the differences between energy computations using RUSLE and RUSLE2 were analyzed. For minute-level data, the ratio of the

245   average kinetic energy computed using RUSLE2 to RUSLE is approximately 1.09, while it is 1.15 for hourly data (Figures 7c and 7d). The analysis was further extended to assess the impact of temporal resolution on *E* and I_{30} calculations. Based on RUSLE's kinetic energy algorithm, results show that values computed from minute-level data are 1.21 times higher than those from hourly data, with more significant differences in the northwest (Figure 7e). The impact on I_{30} is even more pronounced, with minute-level data yielding values 1.72 times higher than those from hourly data (Figure 7f). This analysis

250   highlights that I_{30} values exceed *E* at a national scale and are more sensitive to both temporal resolution of precipitation data

and algorithm selection. Accurate computation of I_{30} is therefore essential for reliable rainfall erosivity estimation, underscoring the importance of high temporal resolution data in achieving precise rainfall erosivity estimates.
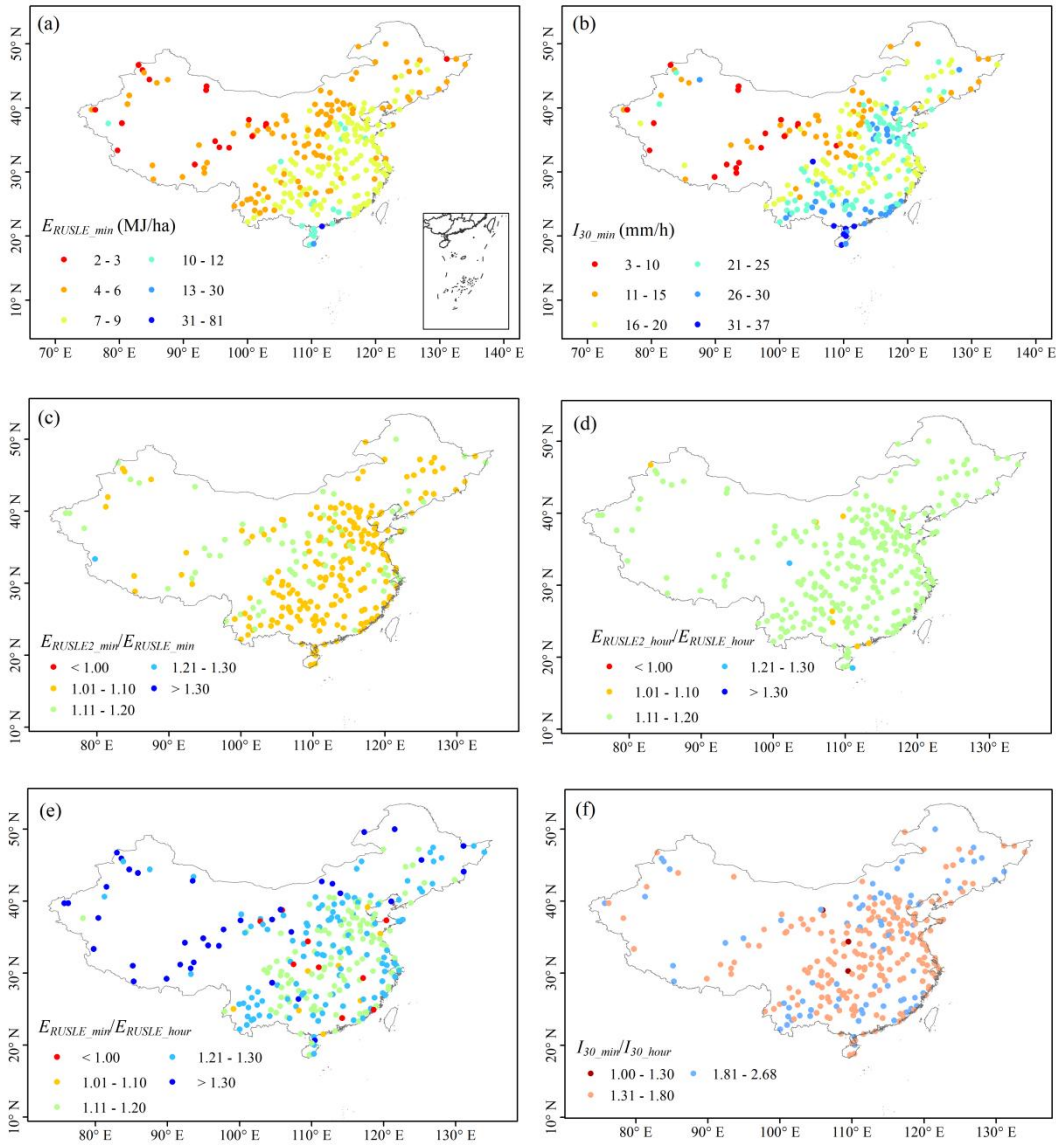
255 **Figure 7: Spatial distribution of (a) mean kinetic energy (E) and (b) maximum 30-minute rainfall intensity (I_{30}) of erosive rainfall events during 2020-2022; (c) Ratio of E calculated using RUSLE and RUSLE2 methods based on 1-minute precipitation data; (d) Same as (c), but for 1-hour data; (e) Ratio of E calculated using the RUSEL method for 1-minute vs. 1-hour data; (f) I_{30} calculated using 1-minute vs. 1-hour data. The subscript "min" indicates results based on 1-minute data, while "hour" refers to 1-hour data. Subscripts "RUSEL" and "RUSLE2" indicate the methods used to estimate E.**

5. Data availability

The dataset is available from the National Tibetan Plateau/Third Pole Environment Data Center (https://doi.org/10.11888/Terre.tpdc.301206; Chen, 2024).

6. Conclusions

The rainfall erosivity of individual rainfall events is determined by two parameters: the E and I_{30}. High spatiotemporal resolution ground precipitation data provides the most accuracy calculations for both E and I_{30}, resulting in the most reliable rainfall erosivity estimates. Accordingly, this study used nearly ten years of 1-minute in-situ precipitation data from 60,129 stations to estimate the R factor across mainland China. The main findings are as follows:

(1) The R factor across mainland China shows significant spatial variability, with a regional average of approximately 1241 MJ·mm·ha^{-1}·h^{-1}·yr^{-1}.

(2) Compared to previous studies, this newly released datasets presents lower mean annual rainfall erosivity values across mainland China by 31%~65%, with significant differences across various river basins.

(3) With current technology, the accuracy of determining I_{30} during erosive rainfall events is much lower that that of E. The main source of deviation in rainfall erosivity estimation is the uncertainty in I_{30}.

This newly developed dataset, based on high-resolution ground precipitation observations from the recent decade, can enhance the accuracy of soil erosion forecasting when combined with other factors in RUSLE/RUSLE2, such as newly released K factor maps (Gupta et al., 2024) and Cover-Management factor. Furthermore, rainfall erosivity can be viewed as a characteristic of rainfall events, offering spatial insights into precipitation-induced disasters in China.

Author contributions

YC designed the study and wrote the manuscript. YX contributed to the methodology. XD and MD contributed to the suggestions for manuscript revision.

Competing Interests

The contact author has declared that neither they nor their co-authors have any competing interests.

Acknowledgments

This research was jointly supported by the National Natural Science Foundation of China (42201156), National Key Research and Development Program of China (2021YFD1500700), and Basic Research Fund of Chinese Academy of

Meteorological Sciences (2023Z004, 2023Z025). Thanks for the Resource and Environmental Science Data Platform for supporting the watershed data in China (https://www.resdc.cn/data.aspx?DATAID=141).

References

290   Agnese, C., Bagarello, V., Corrao, C., D'Agostino, L., and D'Asaro, F.: Influence of the rainfall measurement interval on the erosivity determinations in the Mediterranean area. J Hydrol, 329(1): 39-48, doi:10.1016/j.jhydrol.2006.02.002, 2006.

Angulo-Martínez, M. and Beguería, S.: Estimating rainfall erosivity from daily precipitation records: A comparison among methods using data from the Ebro Basin (NE Spain), J. Hydrol., 379, 111–121, https://doi.org/10.1016/j.jhydrol.2009.09.051, 2009.

295   Ayat, H., Evans, J., Sherwood, S.C., Soderholm, J., Intensification of subhourly heavy rainfall. Science, 378, 655-659. DOI: 10.1126/science.abn8657, 2022.

Borrelli, P., Robinson, D.A., Panagos, P., Lugato, E., Yang, J.E., Alewell, C., Wuepper, D., Montanarella, L., and Ballabio, C: Land use and climate change impacts on global soil erosion by water (2015-2070). P. Natl. Acad. Sci. USA, 117(36): 21994-22001, https://doi.org/10.1073/pnas.2001403117, 2020.

300   Brown, L., Foster, G.: Storm erosivity using idealized intensity distributions. Trans. ASAE, 30, 0379–0386, doi:10.13031/2013.31957, 1987.

Carter, C. E., Greer, J. D., Braud, H. J., and Floyd, J. M. (1974). Raindrop characteristics in south central United States. Trans. ASAE 17, 1033–1037. doi:10.13031/2013.37021

Chen, Y.: A new gridded dataset of rainfall erosivity (1950–2020) in the Tibetan Plateau [dataset], National Tibetan Plateau 305   Data Center, DOI: 10.11888/Terre.tpdc.271833, 2021.

Chen, Y.: The rainfall erosivity in mainland China (2014-2022) [dataset], National Tibetan Plateau Data Center, https://doi.org/10.11888/Terre.tpdc.301206, 2024.

Chen, Y., Ding, M., Zhang, G., Wang, Y., and Li, J.: Evaluation of ERA5 Reanalysis Precipitation Data in the Yarlung Zangbo River Basin of the Tibetan Plateau. J. Hydrometeor., 24: 1491-1507, DOI: 10.1175/JHM-D-22-0229.1, 2023.

310   Chen, Y., Ding, M., Zhang, G., Duan, X., and Wang, C.: The possible role of fused precipitation data in detecting the spatial-temporal pattern of rainfall erosivity over the Tibetan Plateau, China. CATENA, 228, 107114, https://doi.org/10.1016/j.catena.2023.107114, 2023.

Chen, Y., Duan, X., Ding, M., Qi, W., Li, J., and Xie, Y.: New gridded dataset of rainfall erosivity on the Tibetan Plateau. Earth Syst. Sci. Data, 14 (6), 2681-2695, https://doi.org/10.5194/essd-14-2681-2022, 2022.

315   Dai, Q., Zhu, J., Lv, G., Kalin, L., Yao, Y., Zhang, J., and Han, D.: Radar remote sensing reveals potential underestimation of rainfall erosivity at the global scale. Sci. Adv., 9, eadg5551, DOI: 10.1126/sciadv.adg5551, 2023.

Diodato, N., Ljungqvist, F.c., and Bellocchi, G.: Historical predictability of rainfall erosivity: a reconstruction for monitoring extremes over Northern Italy (1500–2019), NPJ Clim. Atmos. Sci., 3, 46, https://doi.org/10.1038/s41612-020-00144-9,

2020.

320   Freitas, E., Coelho, V., Xuan, Y., Melo, D., Gadelha, A., Santos, E., Galvão, C., Filho, G., Barbosa, L., Huffman, G.,
        Petersen, W., Almeida, C.: The performance of the IMERG satellite-based product in identifying sub-daily rainfall events
        and their properties, J Hydrol, 589, 125128, https://doi.org/10.1016/j.jhydrol.2020.125128, 2020.

        FAO & ITPS: Status of the world's soil resources (SWSR) – main report. Food and agriculture Organization of the United
        Nations and Intergovernmental Technical Panel on soils, Rome, Italy. Available online: http://www.fao.org/3/a-i5199e.pdf,
325   2015.

        Gupta, S., Borrelli, P., Panagos, P., Alewell, C., 2024. An advanced global soil erodibility (K) assessment including the
        effects of saturated hydraulic conductivity, Sci. Total. Environ., 908, 168249,
        https://doi.org/10.1016/j.scitotenv.2023.168249.

        Hersbach, H., and Coauthors, 2019: Global reanalysis: Goodbye ERA-Interim, hello ERA5. ECMWF Newsletter, No. 159,
330   ECMWF, Reading, United Kingdom, 17–24, https://doi.org/10.21957/vf291hehd7.

        IPCC: Climate Change and Land: An IPCC Special Report on Climate Change, Desertification,
        Land Degradation, Sustainable Land Management, Food Security, and Greenhouse Gas Fluxes
        in Terrestrial Ecosystems, Cambridge University Press, Cambridge, UK and New York, NY, USA, 896 pp.
        https://doi.org/10.1017/9781009157988, 2019.

335   Kinnell, P.I.A., 1980. Rainfall intensity-kinetic energy relationships for soil loss prediction. Soil Science Society of America
        Proceedings 45, 153-155.

        Laws, J.O., 1941. Measurements of fall-velocity of water-drops and raindrops. Transactions of the American Geophysical
        Union 24, 452.

        Laws, J.O., Parsons, D.A., 1943. The relation of raindrop size to intensity. Transaction of the American Geophysical Union
340   26, 452-460.

        Lim, Y.S.; Kim, J.K.; Kim, J.W.; Park, B.I.; Kim, M.S. Analysis of the Relationship between the Kinetic Energy and
        Intensity of Rainfall in Daejeon, Korea. Quat. Int. 2015, 384, 107–117.

        Liu, B., Xie, Y., Li, Z., Liang, Y., Zhang, W., Fu, S., Yin, S., Wei, X., Zhang, K., Wang, Z., Liu, Y., Zhao, Y., and Guo, Q.:
        The assessment of soil loss by water erosion in China. Int. Soil Water Conse. 8 (4), 430,
345   https://doi.org/10.1016/j.iswcr.2020.07.002, 2020.

        McGuire, L.A., Ebel, B.A., Rengers, F.K., Vieira, D.C.S., and Nyman, P., Fire effects on geomorphic processes, Nat. Rev.
        Earth Env., 5, 486-503, https://doi.org/10.1038/s43017-024-00557-7, 2024.

        Meshesha, D.T., Tsunekawa, A. & Haregeweyn, N. Influence of raindrop size on rainfall intensity, kinetic energy, and
        erosivity in a sub-humid tropical area: a case study in the northern highlands of Ethiopia. Theor Appl Climatol 136, 1221–
350   1231 (2019). https://doi.org/10.1007/s00704-018-2551-0

        Mineo, C., Ridolfi, E., Moccia, B., Russo, F., Napolitano, F. Assessment of Rainfall Kinetic-Energy–Intensity Relationships.
        Water 2019, 11, 1994. https://doi.org/10.3390/w11101994

Nearing, M.A., Yin, S., Borrelli, P., and Polyakov, V.O.: Rainfall erosivity: A historical review. CATENA, 157: 357-362, http://dx.doi.org/10.1016/j.catena.2017.06.004, 2017.

355 Panagos, P., Borrelli, P., Meusburger, K., Yu, B., Klik, A., Lim, K.J., Yang, J.E, Ni, J., Miao, C., Chattopadhyay, N., Sadeghi, S.H., Hazbavi, Z., Zabihi, M., Larionov, G.A., Krasnov, S.F., Garobets, A., Levi, Y., Erpul, G., Birkel, C., Hoyos, N., Naipal, V., Oliveira, P.T.S., Bonilla, C.A., Meddi, M., Nel, W., Dashti, H., Boni, M., Diodato, N., Van, O.K., Nearing, M.A., and Ballabio, C.: Global rainfall erosivity assessment based on high-temporal resolution rainfall records. Sci. Rep.: 7: 4175, DOI: 10.1038/s41598-017-04282-8, 2017.

360 Renard, K.G., and Freimund, J.R: Using monthly precipitation data to estimate the R-factor in the revised USLE. J Hydrol., 157: 287-306, https://doi.org/10.1016/0022-1694(94)90110-4, 1994.

Renard, K.G., Foster, G.R., Weesies, G.A., McCool, D.K., Yoder, D.C., 1997. Predicting Soil Erosion by Water: A Guide to Conservation Planning with the Revised Universal Soil Loss Equation (RUSLE), USDA Agricultural Handbook No. 733. USDA, Washington, DC 384PP..

365 Richardson, C.W., Foster, G.R., and Wright., D.A.: Estimation of Erosion Index from Daily Rainfall Amount. Trans. ASAE, 26(1):153-156, doi:10.13031/2013.33893, 1983.

Tilg, A., F. Vejen, C. B. Hasager, and M. Nielsen, 2020: Rainfall Kinetic Energy in Denmark: Relationship with Drop Size, Wind Speed, and Rain Rate. J. Hydrometeor., 21, 1621 – 1637, https://doi.org/10.1175/JHM-D-19-0251.1

Uijlenhoet, R., Stricker, J.N.M., 1994. A consistent rainfall parameterization based on the exponential raindrop size
370 distribution.Nature reviews earth & environment, 218, 101-127.

USDA-Agricultural Research Service. 2013. Science Documentation Revised Universal Soil Loss Equation Version 2. https://www.ars.usda.gov/ARSUserFiles/60600505/RUSLE/RUSLE2_Science_Doc.pdf.

Wischmeier, W.H., and Smith, D.D.: Predicting rainfall-erosion losses from cropland east of the Rocky Mountains: Guide for selection of practices for soil and water conservation. US 434 Department of Agriculture, 1965.

375 Wischmeier, W.H., and Smith, D.D.: Predicting Rainfall Erosion Losses: A Guide to Conservation Planning, Department of Agriculture, 1978.

Wu, S., Guo, Z., Askar, A., Li, X., Hu, Y., Li, H., and Saria, A.E. Dynamic land cover and ecosystem service changes in global coastal deltas under future climate scenarios. Ocean & Coastal Management, 258, 107384, https://doi.org/10.1016/j.ocecoaman.2024.107384, 2024.

380 Xie, Y., Liu, B.Y., and Zhang, W.B.: Study on standard of erosive rainfall. J. Soil Water Conserv., 14 (4), 6–11, https://doi.org/10.3321/j.issn:1009-2242.2000.04.002, 2000. In Chinese.

Xie, Y., Yin, S., Liu, B., Nearing, M., and Zhao, Y.: Models for estimating daily rainfall erosivity in China. J Hydrol, 535, 547–558, https://doi.org/10.1016/j.jhydrol.2016.02.020, 2016.

Yin, S., Xie, Y., Liu, B., and Nearing, M.A.: Rainfall erosivity estimation based on rainfall data collected over a range of
385 temporal resolutions. Hydrol. Earth Syst. Sci., 19: 4113-4126, doi:10.5194/hess-19-4113-2015, 2015.

Yin, S., Xie, Y., and Wang, C.: Calculation of rainfall erosivity by using hourly rainfall data. Geographical Research, 26(3):

541-547, DOI: 10.11821/yj2007030015, 2007. In Chinese.

Yu, B., and Rosewell, J.C.: Technical Notes: A Robust Estimator of the R-factor for the Universal Soil Loss Equation. Transactions of the ASAE, 39 (2): 559-561, https://doi.org/10.13031/2013.27535, 1996.

390 Yue, T., Yin, S., Xie, Y., Yu, B., and Liu, B.: Rainfall erosivity mapping over mainland China based on high-density hourly rainfall records. Earth Syst. Sci. Data, 14, 665-682, https://doi.org/10.5194/essd-14-665-2022, 2022.